Pharmacogn. Mag.
A multifaceted peer reviewed journal in the field of Pharmacognosy and Natural Products
www.phcog.com | www.phcog.net

ORIGINAL ARTICLE

Green Synthesis-Mediated Iron Oxide Nanoparticles using *Sphagneticola trilobata* (L.) for Antibacterial and Anticancer Assessment

Rakesh Pandit Dhavale, Swapnil Sanjay Patil[1], Sagar Ujwal Jadhav[2], Rushikesh Pandit Dhavale[3], Sachin Bharat Agawane[4]

Departments of Pharmaceutics, [1]Pharmaceutical Quality Assurance and [2]Pharmaceutical Chemistry, Bharati Vidyapeeth College of Pharmacy, Kolhapur, [4]Division of Biochemical Science, National Chemical Laboratory, Pune, Maharashtra, India, [3]Department of Materials Science and Engineering, Yonsei University, 50 Yonsei-ro, Seodaemun-gu, Seoul, 03722, South Korea

Submitted: 30-Jul-2021 Revised: 10-Aug-2021 Accepted: 09-Sep-2021 Published: 23-Nov-2022

ABSTRACT

Background: Green chemistry is widely accepted phenomenon to synthesize iron oxide nanoparticles (Fe-NPs) used in several biomedical and technological applications. Metal oxide nanoparticles are useful in biomedical, clearing environmental pollutants, enzyme immobilization, etc., **Objectives:** The synthesis of Fe-NPs using *Sphagneticola trilobata* leaf extract using ferric chloride solution and its biological assessment. **Materials and Methods:** The present study involved the synthesis of Fe-NPs using *S. trilobata* leaf extract using ferric chloride solution by the co-precipitation method. The synthesized nanoparticles were characterized for Fourier-transform infrared spectroscopy, scanning electron microscopy, powder X-ray diffraction spectroscopy, particle size analysis, and magnetization studies. The nanoparticles were biologically evaluated for microbiological, antioxidant, and *in vitro* cytotoxicity activity. **Results:** Magnetic nanoparticles were appeared in dark brown color. The change in color might result due to the presence of polyphenols in *S. trilobata* leaf extract. The characterization studies confirmed morphology, shape, and size of the nanoparticles. The mean diameter of Fe-NPs and *S. trilobata*-Fe-NPs was found to be 42.2 ± 2.6 and 62.54 ± 2.01 nm, respectively. Magnetization studies of nanoparticles revealed ferromagnetic behavior with the saturation magnetization at 57 emugm^{-1}. *S. trilobata*-Fe-NPs showed significant antibacterial action against *Staphylococcus aureus* and *Bacillus subtilis* by the well-diffusion method. Antioxidant activity of *S. trilobata*-Fe-NPs exhibited 65.78% inhibition in comparison with ascorbic acid. The cytotoxicity assay of *S. trilobata*-Fe-NPs on HCT-15 colon adenocarcinoma cells showed significant anticancer activity (56.44%) cytotoxic inhibition. **Conclusion:** Green synthesis-mediated *S. trilobata*-Fe-NPs appeared to produce significant antimicrobial and anticancer potential.

Key words: Elemental analysis, field emission scanning electron microscopy, green synthesis, iron oxide nanoparticles, *Sphagneticola trilobata,* X-ray diffraction

SUMMARY

- Green synthesis-mediated magnetic nanoparticles (MNPs) from *Sphagneticola trilobata* (L.) leave extract
- Synthesized MNPs were characterized for Fourier transform infrared spectroscopy, field emission scanning electron microscopy, X-ray diffraction, vibrating sample magnetometer, energy-dispersive X-ray spectroscopy, and thermogravimetric analysis
- MNPs were assessed for antibacterial, antioxidant, and *in vitro* cytotoxicity studies.

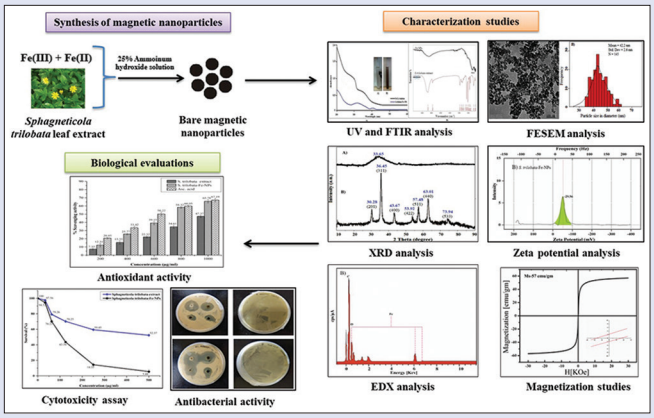

Abbreviations used: Fe-NPs: Iron Oxide Nanoparticles; $FeCl_3.6H_2O$: Ferric chloride hexahydrate; $FeCl_2.4H_2O$: Ferrous chloride tetrahydrate; DPPH: 2,2-Diphenyl-1-picrylhydrazyl; DMEM: Dulbecco's Modified Eagle's Medium; MTT: 3-(4,5-Dimethylthiazol-2-yl)-2,5-Diphenyltetrazolium Bromide; FCS: Fetal Calf Serum; FTIR: Fourier Transform Infrared Spectroscopy; SEM: Scanning Electron Microscopy; XRD: X-ray Diffraction Spectroscopy; HR-TEM: High-Resolution Transmission Electron Microscopy; FESEM: Field Emission Scanning Electron Microscopy; VSM: Vibrating Sample Magnetometer; EDX: Energy-dispersive X-ray spectroscopy; SPR: Surface Plasmon Resonance; TGA: Thermogravimetric analysis; CFU: Colony-Forming Unit; MIC: Minimum Inhibitory Concentration; NCIM: National Collection of Industrial Micro-organisms.

Correspondence:

Dr. Sachin Bharat Agawane,
Division of Biochemical Science, National Chemical Laboratory, Pune, Maharashtra, India.
E-mail: sb.agawane@ncl.res.in

DOI: 10.4103/pm.pm_356_21

Access this article online
Website: www.phcog.com
Quick Response Code:

INTRODUCTION

Iron oxide nanoparticles (Fe-NPs) are synthesized by various processes and received wide scope in nanotechnology. Ferric oxide nanoparticles have enormous applications in the field of medicine, biological sciences, and biomedical engineering.[1] The size of nanoparticles can be controlled either by chemical processes or bioconversion processes. The mean diameter size in the range 100 nm or less possesses unique features.[2] However, nanoparticles synthesized by physical and chemical

Cite this article as: Dhavale RP, Patil SS, Jadhav SU, Dhavale RP, Agawane SB. Green synthesis-mediated iron oxide nanoparticles using *Sphagneticola trilobata* (L.) for antibacterial and anticancer assessment. Phcog Mag 2022;18:953-61.

methods offer definite properties such as thermal, catalytic, electrical conductivity, and optical properties[3] but implicit toxicity and cost unproductive.[4,5] Nanoparticles are synthesized either by top to bottom or bottom to top approaches,[6] in controlled size and shape.[7] The properties of nanoparticles are unique due to better ratio of surface to volume and high surface energy. These properties are well correlated with the sizes of nanoparticles. The size of nanoparticles and toxicities can be controlled by various processes along with essential polymeric media.[8]

Nanoparticles are widely used as an anticancer, antimicrobial,[9] antiplasmodial,[10] larvicidal,[11] mosquitocidal,[12] to control tropical disease such as malaria, dengue, and filariasis.[12] Fe-NPs are widely used in biomedical applications in surface chemistry to generate biosensors, in cell sorting and tissue repairment, detoxification of biological fluids, hyperthermia,[13] magnetic resonance imaging in cancer diagnostics,[14] thernoustics,[15] and targeted drug delivery.[16,17] The various strategies are initiated in the design of nanoparticles by green chemistry protocols used to control cancerous growth, being comparatively less toxic carriers.[18] Currently, cancer thernoustics act promising therapies against cancerous cells than normal cells, with aim to reduce toxicity and multiple drug resistance.[19] Nanoparticles as drug carriers have achieved a promising role in coordinating proper interactions between enzymes, receptors, antibodies with cancer cells; thus assisting proper diagnosis and cancer therapy.[20] The single step synthesis of nanoparticle has achieved greater technological applications such as removal of pollutants from water,[21,22] battery performance,[23] photocatalysis,[24] and high-performance dye sensitized solar cells.[25] Fe-NPs are synthesized by sol–gel reactions,[26] hydrothermal methods,[27] flow injection synthesis,[28] sonochemical,[29,30] microwave methods,[31] aerosol pyrolysis,[32] radiolysis,[33] microemulsion process,[34] and laser pyrolysis.[35] The physical and chemical methods useful in the synthesis of nanoparticles are screened based on the parameters such as effective and controlled size, loss of reactivity in alteration of magnetism, aggregation of air exposure,[36] and dispersibility.[37] The use of chemical synthetic processes generates products with contaminated toxic chemicals, precursors, and byproducts.[38] Thus, an attempt was made to synthesize metal or metal oxide nanoparticles by clean, simple, inexpensive, environmentally friendly method using plant extract. The microbial cultures, mushrooms, and algae are also used to produce nanoparticles with greater stability. The stability of nanoparticles can be achieved with reference to the organic content present in plant extracts. Further, advantages of green synthesis over chemical synthesis in nanoparticles synthesis lies in the parameters such as cost, time, and complex steps. Further, nanotechnology has facilitated nanoparticles for improved therapeutic delivery of antibiotic and nonantibiotic antimicrobial agents by virtue of bypassing bacterial resistance mechanisms. However, the development in nanotechnology has restricted their use due to improper size control with available processes. Thus, the stabilization and size of nanoparticles may be controlled using such constituents obtained from the plants. Many scientists have successfully attempted to prepare nanoparticles using extracts, namely *Artemisia annua* leaf extract,[39] *Perilla frutescens* leaf extract,[40] *Caricaya papaya,*[41] plantain peel extract,[42] and *Kappaphycus alvarezii* seaweed extract,[43] for catalytic, anti-inflammatory, and antimicrobial potential.[44] The mechanism of formation of stable Fe-NPs followed bioreduction of ferric ions by polyol components and water soluble heterocyclic components in the plant extract.

Sphagneticola trilobata, family *Asteraceae*, is herbaceous perennial plant. The stems are more or less prostrate, forming new roots at the leaf nodes. The strong decoction of the whole plant can be effective to treat severe chest colds. In combination with *Lantana camara*, *Commelina nudiflora*, *Hibiscus sabdariffa* and *Citrus aurantiifolia* as a tea or syrup is an excellent remedy for colds. *S. trilobata* is harvested for local medicinal use and cultivated as an ornamental ground cover. The plant is largely found in India, China, Mexico, Central America, the Caribbean, Hong Kong, South Africa, Australia, Indonesia. The leaves of *S. trilobata* are effective for arthritic pain, backache, musclespasms, rheumatism, wounds, sores, and swellings.[45] Aqueous extracts of *S. trilobata* have shown promising inhibition over streptozotocin-induced hyperglycemia in rats.[46] Major constituents present in oil were α-pinene, α-phellandrene, sabinene, limonene, β-pinene, camphene, germacrene D, and γ-amorphene.[47] Apart, the whole plant of *S. trilobata* contains lignans and phenolic glycosides.[48] The flower extracts of *S. trilobata* were used to synthesize silver nanoparticles using the green synthesis for antibacterial activity.[49] The present study aimed to synthesize Fe-NPs with greener and ecofriendly method using aqueous extract of *S. trilobata*. The prepared *S. trilobata* magnetic nanoparticles (MNPs) are further investigated for antimicrobial and anticancer activities using bacterial cultures and cancer cell line.

MATERIALS AND METHODS

Materials

Ferric chloride hexahydrate ($FeCl_3.6H_2O$), ferrous chloride tetrahydrate ($FeCl_2.4H_2O$, 99%) and 2,2-Diphenyl-1-picrylhydrazyl (DPPH) were purchased from Sigma Aldrich. Dulbecco's Modified Eagle's Medium, trypsin and 3-(4,5-Dimethylthiazol-2-yl)-2,5-Diphenyltetrazolium Bromide (MTT) were purchased from Himedia, Mumbai. HCT-15 colon adenocarcinoma cell line was obtained from National Center for Cell Sciences, Pune. All other reagents of analytical grades were used for further experimentation. The leaves of *S. trilobata* collected were collected from CSIR-NCL, Pune. The plant received authentication from Botanical Survey of India, Pune. The plant was authenticated as *S. trilobata* (L.) Pruski family *Asteraceae* with authentication number BSI/WRC/IDEN. CER./2018/H3. The leaves were washed two to three times with deionized water. All glasswares were cleaned with nitric acid mixture and double distilled water.

Preparation of plant extract

S. trilobata leaves were thoroughly washed with deionized water and kept for sun dried. The leaves were finely grounded to powdered form and stored in the glass bottle at the room temperature. Extraction process was initiated in the conical flask containing 10 mg finely leaf powder mixed in 100 mL double-distilled water on water bath at the constant temperature 80°C. The mixture was allowed to filter through Whatmann no. 2 filter paper.[50,51] The obtained leaf extract was kept at 4°C in dark place for future use.

Sphagneticola trilobata iron oxide nanoparticles (*Sphagneticola trilobata*-iron oxide nanoparticles) synthesis

Fe-NPs were synthesized by the coprecipitation method.[52] The measured amount of Fe^{2+} and Fe^{3+} in molar ratio 1:2 was added in double distilled water under continuous stirring at 400 rpm for 25 min. Further, 3 mL, 25% ammonium hydroxide solution was added in above mixture and stirred continuously at 1500 rpm at 80°C for 1 h. The later synthesis of Fe-NPs was followed by the addition of *S. trilobata* leaf extract in iron solution which was used as precursor. *S. trilobata* leaf extract; 50 mL, was dropped slowly in 100 mL 0.1 mM iron solution (1:2) under constant stirring at the room temperature. Further, the reaction was processed with addition of 3 mL, 25% ammonium hydroxide

solution in *S. trilobata*/Fe^{3+} suspension under continuous stirring till visible yellow color aqueous iron solution turned to dark brown within 5 min. The mixture was stirred for 1 h and kept undisturbed for next 30 min, centrifuged, washed several times with distilled water and dried overnight under vacuum to obtain the *S. trilobata*-Fe-NPs. The prepared nanoparticles were further used for characterizations[53] and biological applications.

Characterizations

S. trilobata-Fe-NPs were monitored by ultraviolet visible (UV-Vis) spectrophotometer (UV-530, JASCO). The bioreductive property of aqueous *S. trilobata* extracts was determined by considering temperature as its function. Magnetization measurements of nanoparticles verses field loop were measured using vibrating sample magnetometer (VSM) (Quantum Design, Inc.) at 300 K in the magnetic field. *S. trilobata*-Fe-NPs were analyzed for Fourier transform infrared spectroscopy (FTIR) studies to reveal the presence of functional groups. The dried nanoparticles were formed in KBR pellets for FTIR analysis using plain KBr pellets as a reference for background correction. The characteristic infrared absorption spectra of *S. trilobata* -Fe-NPs and *S. trilobata* extract were recorded using a FTIR (Bruker). The spectra were obtained in the diffuse reflectance mode at 4 cm^{-1} resolution. The morphological features of *S. trilobata* -Fe-NPs were studied by scanning electron microscopy (QUANTA-200-3D, FEI, USA) at 20.0 KV. Field emission scanning electron microscope (FESEM) JEOL JSM-6360 was employed to study the surface morphology and particle size investigations. The morphological and size distribution of Fe-NPs was done using high-resolution transmission electron microscopy (HR-TEM) JEM-2100F. The *S. trilobata* -Fe-NPs were observed for elemental analysis, X-ray spectroscopy using Shimadzu EDX700HS spectrometer. Zeta potential studies were conducted to measure the charge on the surface of droplet for confirmation of stability of *S. trilobata*-Fe-NPs. X-ray diffraction (XRD) measurements were performed on Bruker AXS D2 phaser diffractometer. XRD patterns were recorded from a thin film of powdered nanoparticles using analytical "X"pert-pro system at a scan rate 0.25 step/sec. The powdered sample was exposed to Cu-Kα radiation and the diffraction pattern was analyzed from 7° to 80° (2 θ) with a step size of 0.02°. Debye-Scherrer equation was applied to count the average particle size of MNPs to correlate peak broadening with particle size.

$$d = k\lambda/(\beta \cdot \cos\theta). \quad \text{Eq. no. 1}$$

where, "*d*" is the particle size, "*k*" is the Scherrer constant (0.9), "λ" is the X-ray wavelength (0.15406 nm), "β" is the width of the XRD peak at half-height and "θ" is the Bragg diffraction angle. Thermogravimetric analysis of Fe-NPs was done using a TGA 5000IR at 10°C/min in nitrogen (10 mL/min.)

Culturing bacterial strains

Bacterial strains Gram positive, namely *Escherichia coli* NCIM 2065, *Pseudomonas aeruginosa* NCIM 2200, and Gram negative viz., *Bacillus subtilis* NCIM 2063, *Staphylococcus aureus* NCIM 2079 were procured from National Center for Industrial Micro-organisms (NCIM, NCL, Pune, Maharashtra, India). The bacterial cells were cultured in nutrient broth and used as inoculum. Inoculums were homogenized, centrifuged, and adjusted to 0.5 McFarland standards (5×10^5 CFU/mL).

Antibacterial activity

The antibacterial activity of *S. trilobata* and *S. trilobata* -Fe-NPs was evaluated by the cup plate method. Agar plates were inoculated with 100 µL, 24 h freshly cultured viable bacterial cells (1.0×10^7 colony-forming units) by the spread plate method. The dried plates were bored to form 5 mm diameter wells using a sterile cork borer. *S. trilobata* -Fe-NPs at concentrations, 100 and 250 µg/mL and *S. trilobata* extract, each 100 µL, were introduced into the bored well. The plates were kept in incubator at 37°C for 24–48 h. The antibacterial activity was measured by determining the zone of inhibition using the zone reader.

Minimum inhibitory concentration determinations

The minimum inhibitory concentration (MIC) of *S. trilobata*-Fe-NPs was determined by broth microdilution method using 96-well microtiter plates. Aliquots of *S. trilobata*-Fe-NPs 100 µL, in concentrations (µg/mL) as 100.00; 75.00; 37.50; 18.75; 9.37; 4.69; 2.34; 1.17; 0.59; 0.29 were placed in sterile 96-well plates. The microtiter plate was allowed to incubate for 24 h at 37°C. MIC was said to the lowest concentration at which no visible growth was observed. Dimethyl sulfoxide and Mueller–Hinton broth were used as controls. In control experiments, cells were incubated with only 10 mM sodium phosphate buffer. Ciprofloxacin was used as a positive control. The results were analyzed in replicates per assay.

Antioxidant activity

Antioxidant activity of the *S. trilobata* extract and *S. trilobata* -Fe-NPs was determined as per free radical scavenging property.[54] Briefly, the reaction mixture contained 1 mL 0.135 mM DPPH in methanol and 2 mL, aqueous solutions of *S. trilobata* extract and *S. trilobata* -Fe-NPs in concentrations from 200 µg/mL to 1000 µg/mL and set out in in dark for 30 min at 37°C. The absorbance was taken at 517 nm using UV spectrophotometer (Spectrama × 340, Molecular Devises). Percentage scavenging effect was determined in comparison with a standard ascorbic acid using equation:

% scavenging effect = ([Abs. of control − Abs. of test sample]/Abs. of control) ×100. Eq. no. 2

Where, Abs. of control was the absorbance of DPPH radical with methanol; Abs. of test sample was the absorbance of DPPH radical with *S. trilobata* extract.

In vitro cytotoxicity assay

HCT-15 colon adenocarcinoma cell line was maintained in flasks with 10% (*v/v*) fetal calf serum containing Roswell Park Memorial Institute medium 1640 in a humidified atmosphere containing 5% CO_2. The extracts were prepared in the concentration as 100 µg/mL to 1.56 µg/mL and tested for cytotoxicity using MTT assay on HCT-15 colon adenocarcinoma cell line. The 80% confluent cells were trypsinized and observed for cell viability through inverted phase microscope (FusionTek, India). The 1×10^5 cells were seeded in a 96 well plate and incubated overnight in a humidified atmosphere containing 5% CO_2. Next day, cells were treated with 100, 50, 25, 12.5, 6.25, 3.12, and 1.5 µg/mL extract, incubated for 48 h. After incubation, medium was replaced with 0.5 mg/mL MTT and incubated for 4 h to form reduced formazan crystals which were further solubilized in acidified isopropanol. The change in color was recorded by measuring the optical density on a microplate reader (BioRad) at 570 nm against a blank. DMSO treated cells were observed to be 100% cell growth. Thus, the percentage cytotoxicity was determined as

$$\% \text{ Cytotoxicity} = \frac{(\text{Absorbance of control} - \text{Absorbance of extract})}{\left(\text{Absorbance of control} - \text{Absorbance of blank}\right)} \times 100 \quad \text{Eq. no. 3}$$

where DMSO treated cells were acted as control and medium deprived cells was considered as a blank.

RESULTS AND DISCUSSION

Bioreduction process of *Sphagneticola trilobata*-Fe-NPs

Ferrous and ferric chloride solutions as iron precursor were added in *S. trilobata* leaf extract. Fe-NPs were achieved by reduction of ferric ions with polyols containing hydroxyl and aldehyde groups present in leaf extract in alkaline condition. Ferric chlorides hydrolyze to form ferric hydroxide and released hydrogen ions. Further, ferric hydroxide was partially reduced by the *S. trilobata* leaf extract to form Fe-NPs, while aldehyde groups oxidized to the corresponding acids which confirmed the mechanism of Fe-NPs synthesis. The rapid change in the color of extract solutions from yellow to dark brown at the room temperature resulted in the formation of *S. trilobata* -Fe-NPs. Thus, the reliable, nontoxic, and ecofriendly method was implemented for the synthesis of nanoparticles to avoid participation of residual chemicals.

Ultraviolet-visible spectroscopy

The optical, photocatalytic, and stability of Fe-NPs synthesized using *S. trilobata* extracts were initially examined by UV-Vis spectrometric analysis to monitor the peak of reduced ferric oxide nanoparticles in aqueous solution.

The UV-Vis spectroscopic analysis revealed the distinct surface plasmon resonance band at 320 nm characteristic feature of spherical *S. trilobata*-Fe-NPs, [Figure 1a]. Reduction of Fe^{3+}-Fe^{2+} solution by *S. trilobata* leaf extract within 3 h was indicated by visual color change to stable brown and indicated the formation of *S. trilobata*-Fe-NPs

Fourier-transform infrared spectroscopy

The interactions between the *S. trilobata* extracts, Fe^{3+} precursor, and Fe-NPs were confirmed by FTIR. FTIR spectra of the *S. trilobata*-Fe-NPs in [Figure 1b] showed the presence of vibration band at 584 cm^{-1} (C-I stretching) characteristic feature of Fe_3O_4 formation. Further, FTIR spectrum of the extract showed peaks at 910 cm^{-1} (C = C bending) monosubstituted alkene, 1020 cm^{-1} (C–N stretching) amines, 1373 cm^{-1} (O-H bending) phenols, 1324 cm^{-1} (C–N stretching) aromatic amines, 2935 cm^{-1} (C–H stretching) alkane and a broad peak at 3190 cm^{-1} (O-H stretching) alcohol [Figure 1b]. The bands obtained for the various functional groups represented metabolites of leaf extract. The distinct IR bands correspond to alcohol, amines, phenols, and carbonyl functional groups. The presence of high content of phenolic compounds in *S. trilobata* leaf extract may lead to show strong antioxidant activity

Magnetization measurements

The magnetization measurement of the *S. trilobata* -Fe-NPs was examined by VSM at 300 K. Magnetic characterization of the *S. trilobata*-Fe-NPs (1.0 g) was represented by the magnetization curves with high saturation magnetization (Ms) 57.0 $emugm^{-1}$ and low coercivity 32.45 Oe. Thus, Fe-NPs formed due to *S. trilobata* extract were found to be high saturation magnetization (Ms). Magnetic hysteresis defines the lag or delay of magnetic materials which relates to the materials in magnetized and demagnetized forms. Hysteresis graph for *S. trilobata* -Fe-NPs showed measurements of magnetic field in range 50 Oe to + 50 Oe, as shown in Figure 2 with coercivity (Hc), as 32.45 Oe and indicated the synthesized *S. trilobata* -Fe-NPs get rapidly attracted toward an external permanent magnet. The nanoparticles get easily dispersed after the removal of the magnet.

Morphological study and particle size distribution

Fe-NPs and *S. trilobata*-Fe-NPs were synthesized by co-precipitation method showed the agglomeration of Fe-NPs in cubic nature Figure 3a and c. The histogram of distribution of particle size was represented in histogram revealed mean size of nanoparticles count. The mean size of Fe-NPs and *S. trilobata* -Fe-NPs was found as 42.2 ± 2.6 nm and 62.54 ± 2.01 nm Figure 3b and d, respectively. Microscopic images revealed the fabrication of smaller nanoparticles in reduced agglomerated form which is as an indication of *S. trilobata* functional group interaction effect on the surface of nanoparticles. The cubic structures of nanoparticles evidenced from HR-TEM determine the influence of an extract on the size of nanoparticles. The electron diffraction pattern of *S. trilobata* -Fe-NPs and HR-TEM image confirm crystalinity with the lattice spacing measured as 0.35 nm [Supplementary Figure S1]. The "d spacing" values between the lattice of iron nanoparticles agreed with the earlier reports.[55] Further, FESEM analysis showed the spherical structure of nanoparticles and crystallite size as 42.2 nm obtained from the histogram of the *S. trilobata*-Fe-NPs. Thus, the size of nanoparticles was significantly controlled by reduction of Fe^{3+}-Fe^{2+} solution by *S. trilobata* leaf extract as evidenced from XRD and FESEM analysis

FESEM and Energy-dispersive X-ray spectroscopy (EDX) analysis depicted spherical morphology [Figure 4a] and presence of iron in the nanoparticles [Figure 4b]. However, MNPs were appeared in the agglomerated state due to hydroxyl content on the MNPs surface. EDX

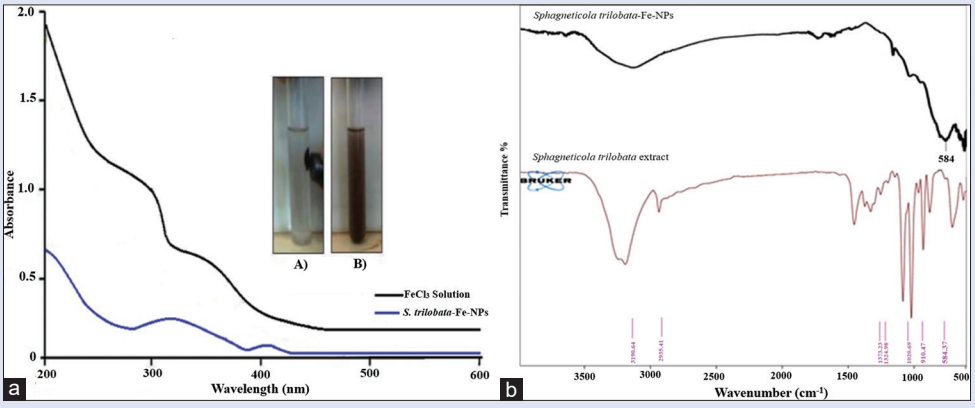

Figure 1: Ultraviolet spectrum of Ferric chloride solution and *Sphagneticola trilobata*- iron oxide nanoparticles with inset diagram, separated magnetic nanoparticles (a) from the reaction mixture by external magnet and dispersed magnetic nanoparticles (b); Fourier-transform infrared spectroscopy spectra of *Sphagneticola trilobata*-iron oxide nanoparticles and *Sphagneticola trilobata* extract

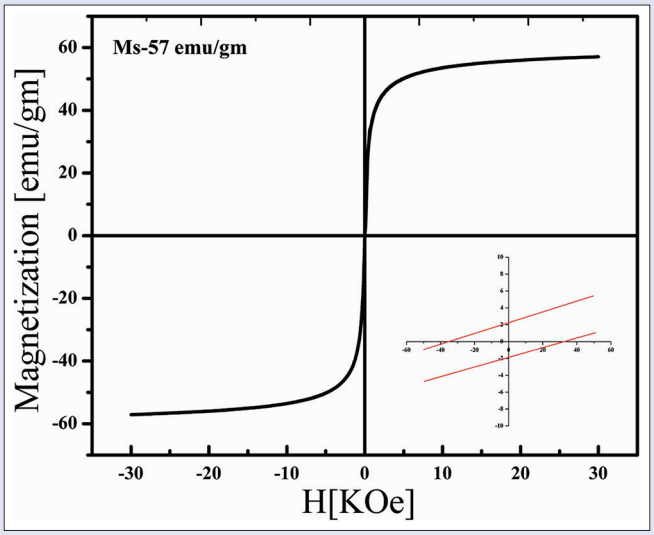

Figure 2: Magnetization curve of the *Sphagneticola trilobata*–iron oxide nanoparticles and inset diagram, Hysteresis graph of *Sphagneticola trilobata*-iron oxide nanoparticles showing magnetic field measurement and coercivity

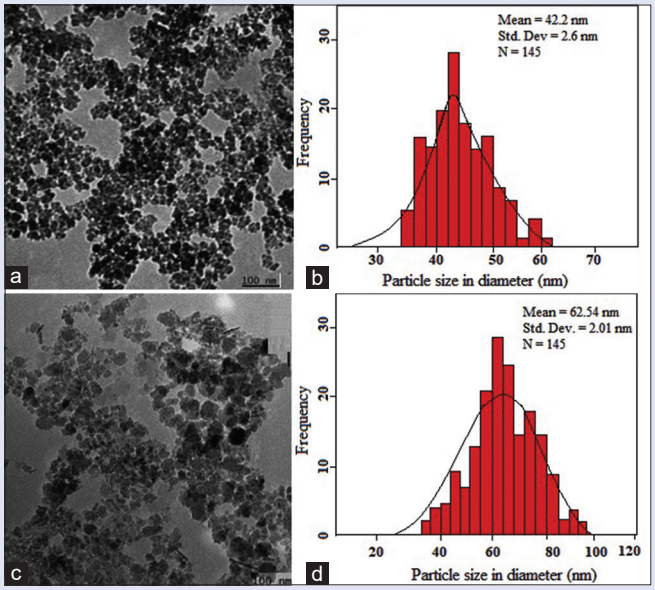

Figure 3: Field emission scanning electron microscope analysis of the agglomeration of (a) iron oxide nanoparticles and (c) *Sphagneticola trilobata*-iron oxide nanoparticles and mean size of (b) iron oxide nanoparticles and (d) *Sphagneticola trilobata*-iron oxide nanoparticles

showed the presence of iron element with its unique atomic structure and chemical composition in *S. trilobata* -Fe-NPs. The identification of elements in the compound was determined as per the amplitude of the peaks obtained in reflected X-rays. According to EDX, the peak amplitude in the range 0.7–7 keV confirmed the presence of iron elements. From the EDX spectra, the identified areas in the particles (0.7, 6.3, and 7.0) represented iron peaks demonstrated increased percentage of iron

Zeta potential measurement determines the stability of the nanoparticles in long-term based on charges on the surface. The stabilization of nanoparticles by the repulsion of electrostatic interactions was indicated in terms of a zeta value ± 30 mV. The zeta value ± 20 mV was also sufficient, when combined with electrostatic and steric stabilization. Zeta potential measurements for *S. trilobata* and *S. trilobata* -Fe-NPs showed -27.04 mV and -29.56 mV at room temperature. The zeta values were sufficient for the stability of the solution, which was achieved as per requirement, whereas the magnetization measurements were not affected due to reduced zeta value [Figure 5].

Powder X-ray diffraction analysis

XRD spectrum, as shown in Figure 6a, *S. trilobata* extract represented a broad diffraction peak at 33.65°. The interactions of polyphenolic constituents of extract on surface of iron nanoparticles was determined with slightly decreased intensity or shifting of the peak as observed in XRD spectrum. However, XRD patterns of *S. trilobata*-Fe-NPs, as shown in Figure 6b, showed existence of strong diffraction peaks with 2 θ values of 30.28°, 36.45°, 43.67°, 53.92°, 57.48°, 63.01°, and 73.94° correspond to the crystal planes of (2 0 1), (3 1 1), (4 0 0), (4 2 2), (5 1 1), (4 4 0), and (5 3 3) confirm *S. trilobata* -Fe-NPs in cubic structure. Based on the Debye-Scherrer equation, a good relationship between the broadening of XRD peak and crystallite size crystallite size of synthesized *S. trilobata*-Fe-NPs was obtained. The crystallite mean size of *S. trilobata*-Fe-NPs was found to be 12.36 nm, calculated in consideration with the full-width of the *S. trilobata*-Fe-NPs diffraction peak at all 2 θ. Further, XRD pattern determined high purity crystalinity of synthesized *S. trilobata*-Fe-NPs.

Thermogravimetric analysis

Thermogravimetric analysis of Fe-NPs and *S. trilobata* -Fe-NPs showed a slight weight loss in the 30°C–100°C. The loss may be accompanied due to the presence of moisture content in the sample. As per thermogram, transformation of Fe_3O_4 to γ-Fe_2O_3 and Fe_2O_3 to α-$Fe_2O_3$3 was observed from 100°C to 800°C. Similarly, a change in the mass profile was observed over 100°C–350°C [Figure 7]. The final weight loss of Fe-NPs and *S. trilobata* -Fe-NPs was found to be 93.58% and 87.43%, respectively.

Antibacterial activity

The antibacterial activity of *S. trilobata* aqueous extract and *S. trilobata* -Fe-NPs on bacterial pathogens, *S. aureus* and *B. subtilis* showed considerable zone of inhibition. The antibacterial activity of *S. trilobata* -Fe-NPs by the well-diffusion method showed 2.8 cm and 3.9 cm zone of inhibition at 100 µg/mL, as shown in Table 1 against *S. aureus* and *B. subtilis,* respectively. The antibacterial activity of *S. trilobata* aqueous extract was observed low against these bacterial strains in comparison to *S. trilobata* -Fe-NPs [Supplementary Figure S2]. MIC experiment demonstrated that *S. trilobata*-Fe-NPs were effective against *S. aureus* and *B. subtilis* at 100 µg/mL. The MIC value of *S. trilobata*-Fe-NPs was found less compared with Ciprofloxacin, 0.7 µg/mL and 0.1 µg/mL against *S. aureus* and *B. subtilis,* respectively. The presence of chemical constituents bearing hydroxyl, sulfate and phenolic compounds along with iron oxide functionality resulted in greater antibacterial activity against above pathogens. Thus, the determination of MIC for *S. trilobata*-Fe-NPs against *S. aureus* and *B. subtilis* was achieved at 100 µg/mL. *S. trilobata* -Fe-NPs exhibit improved therapeutic activity by inhibitory action against various micro-organisms. The killing effect is exerted through microbial cell interactions either directly or indirectly by penetrating in cell envelopes, iron and heavy metal accumulation, acting as a potent carriers and interrupting electron transfer mechanisms.

Table 1: Antibacterial activity of *Sphagneticola trilobata* leaf extract and *Sphagneticola trilobata*-iron oxide nanoparticles

Pathogenic bacteria Zone of inhibition (cm)	*S. trilobata* leaf extract	*S. trilobata*–Fe-NPs (100 µg/mL)	*S. trilobata*–Fe-NPs (75 µg/mL)	Dimethyl sulfoxide
S. aureus	1.1	2.8	1.8	0.5
B. subtilis	2.5	3.9	3.3	0.5

S. trilobata: *Sphagneticola trilobata*; Fe-NPs: Iron oxide nanoparticles; *S. aureus*: *Staphylococcus aureus; B. subtilis*: *Bacillus subtilis*

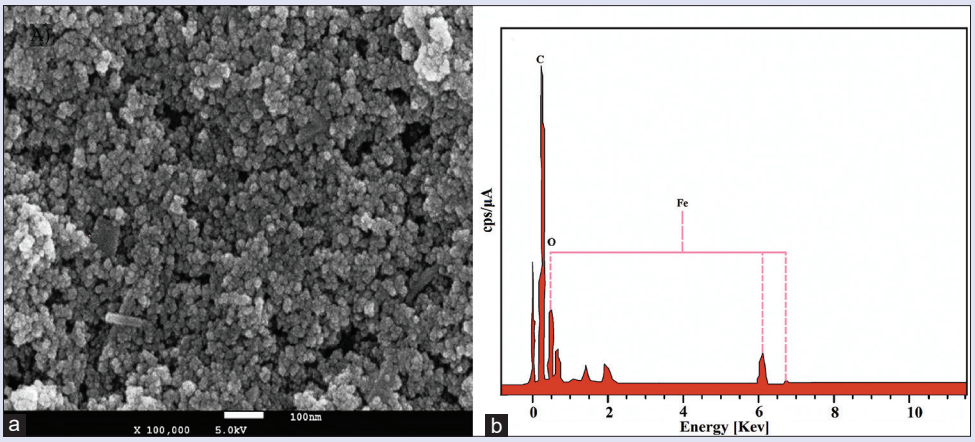

Figure 4: (a) Field emission scanning electron microscope analysis of nanoparticle size distribution and (b) Energy-dispersive X-ray spectroscopy analysis of *Sphagneticola trilobata*-iron oxide nanoparticles to identify element composition

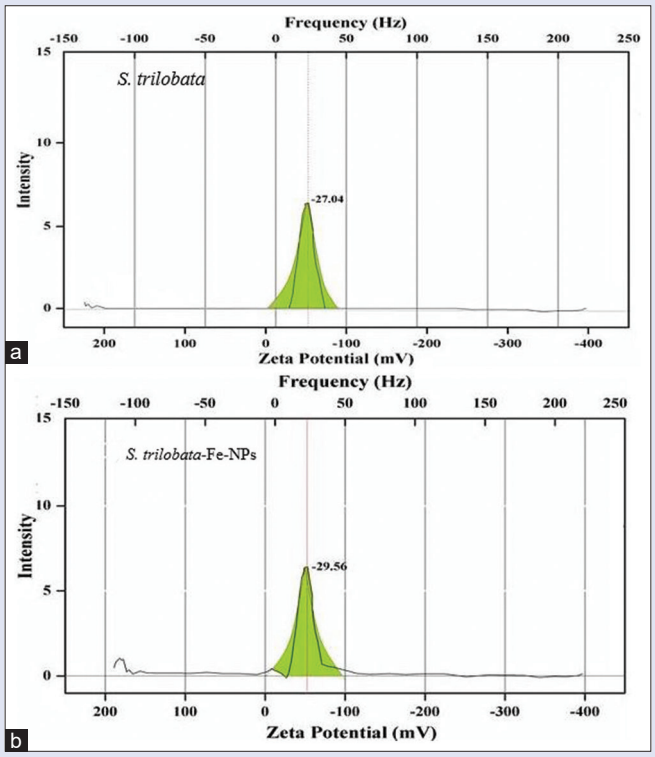

Figure 5: Zeta potential measurement of (a) *Sphagneticola trilobata* and (b) *Sphagneticola trilobata*-Fe NPs

Antioxidant activity

Antioxidant activity of the *S. trilobata* extract and *S. trilobata* -Fe-NPs was determined by DPPH assay. DPPH is stable free radical used as an electron acceptor and generates hydrogen free radical to react with Fe^{3+} to form a stable diamagnetic molecule.[54] The maximum scavenging effect, 65.78% was observed for *S. trilobata* -Fe-NPs at 1000 µg/mL in comparison to ascorbic acid [Figure 8]. The scavenging activity was raised with increase in concentration of *S. trilobata* extract and *S. trilobata* -Fe-NPs. The scavenging effects of samples above 50% were found at 600–1000 µg/mL. The presence of constituents in *S. trilobata* containing polyphenols may be responsible for greater antioxidant potential as observed on account of oxidation of free radicals.

In vitro cytotoxicity assay

Cytotoxicity studies of the *S. trilobata* extract and *S. trilobata* -Fe-NPs investigated on HCT-15 colon adenocarcinoma cells were conducted at various concentrations 32.75 µg/mL to 500.0 µg/mL, incubated at 37°C for 72 h. MTT assay revealed at 500.0 µg/mL and 125.0 µg/mL showed 94.52% and 56.44% cytotoxic inhibition, respectively, [Figure 9]. Thus, IC_{50} value of *S. trilobata* -Fe-NPs was obtained as 125.0 µg/mL. The previous study of starch functionalized iron oxide nanoparticles were found to be non-toxic for normal and cervical cell lines.[56] Supplementary Figure S3 showed the cytotoxic effect of presence and absence of *S. trilobata*-Fe-NPs on cells. The HCT-15 colon adenocarcinoma cells appeared to be adherent. However, the cells were disrupted after the effect of *S. trilobata*-Fe-NPs as represented in Supplementary Figure S3. The polyphenols as active constituents in *S. trilobata* like viz., pinoresinol, pinoresinol-4-sulphate and pinoresinol-4-O-ß-D-glucopyranoside, 1H-indole-3-carboxylic acid, etc., may possess anticancer potential which essentially needs to be elucidated for further investigation.

CONCLUSION

Fe-NPs were synthesized using economical, efficient, and eco-friendly process using *S. trilobata* extract. *S. trilobata* -Fe-NPs were characterized using UV–visible spectroscopy, XRD, FTIR, and FESEM. *S. trilobata* -Fe-NPs were found active against *S. aureus* and *B. subtilis* and showed prominent zone of inhibition. The free radical scavenging activity of *S. trilobata* -Fe-NPs indicated potential antioxidant activity.

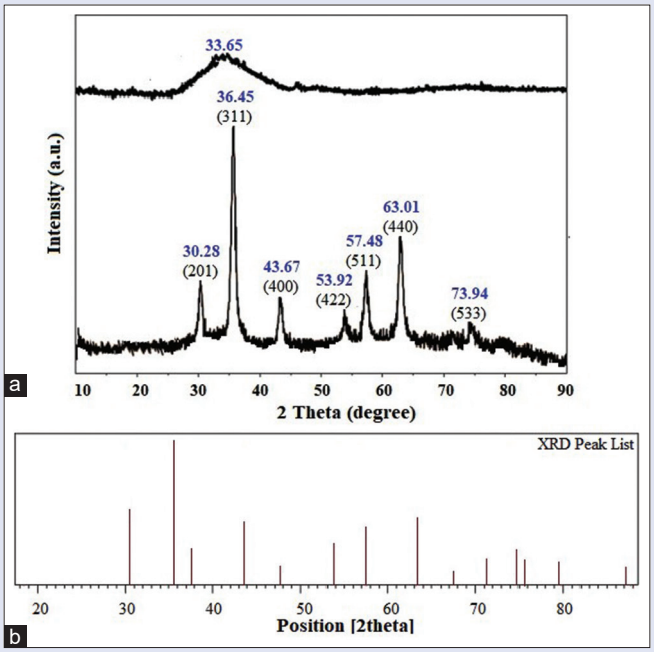

Figure 6: X-ray diffraction spectrum (a) *Sphagneticola trilobata* extract with broad diffraction peak (b) *Sphagneticola trilobata*- iron oxide nanoparticles with strong diffraction peaks

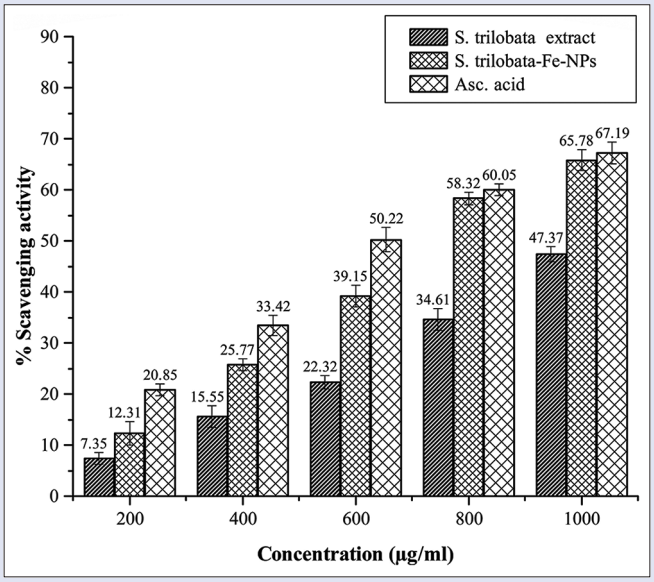

Figure 8: Antioxidant activity of *Sphagneticola trilobata* extract and *Sphagneticola trilobata*-iron oxide nanoparticles by 2,2-Diphenyl-1-picrylhydrazyl assay

The anticancer activity of *S. trilobata*-Fe-NPs on HCT-15 colon adenocarcinoma cells proved beneficial targeting colon cancer. The role of active constituents in plant extracts helped to control nanoparticle size, thereby attracted many scientists in developing MNPs. Thus, it has become an integral part in synthesis of nanoparticles, whereby the stabilization and adsorption property to hold drug and other constituents is predominantly increased. Thus, such approach may ensure the reduction in time and cost expenditure in the preparation of nanoparticle synthesis.

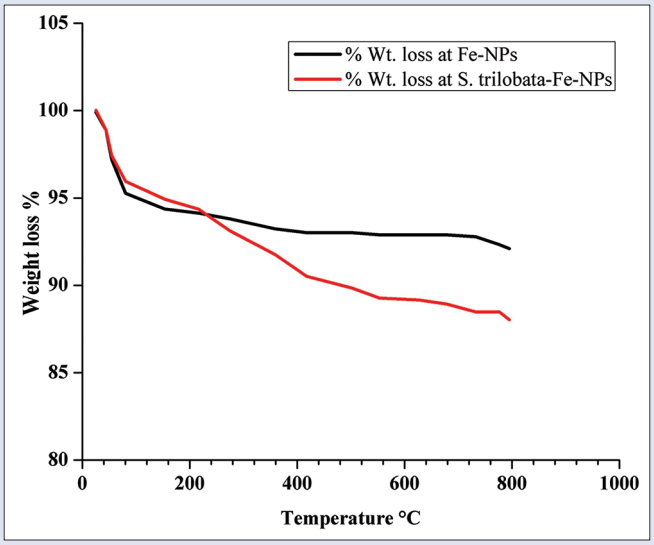

Figure 7: Thermogravimetric analysis of iron oxide nanoparticles and *Sphagneticola trilobata*-iron oxide nanoparticles with corresponding weight loss

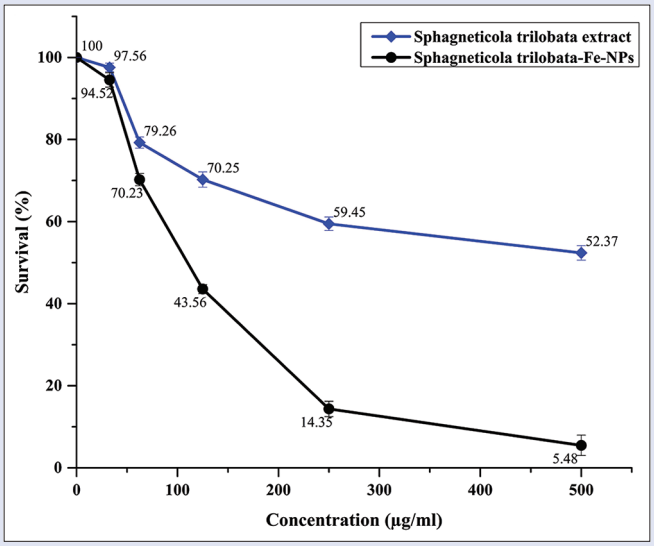

Figure 9: Cytotoxicity assay of *Sphagneticola trilobata* extract and *Sphagneticola trilobata*- iron oxide nanoparticles on HCT-15 colon adenocarcinoma cells

Acknowledgements

The authors are thankful to the Director, CSIR-National Chemical Laboratory, Pune, India, for particle size, Zeta potential, SEM, and XRD analysis.

Financial support and sponsorship

Nil.

Conflicts of interest

There are no conflicts of interest.

REFERENCES

1. Albrecht MA, Evans CW, Raston CL. Green chemistry and the health implications of nanoparticles. Green Chem 2006;8:417-32.

2. Darezereshki E, Ranjbar M, Bakhtiari F. One-step synthesis of maghemite (γ-Fe2O3) nano-particles by wet chemical method. J Alloys Compd 2010;502:257-60.
3. Shameli K, Ahmad MB, Jazayeri SD, Sedaghat S, Shabanzadeh P, Jahangirian H, *et al.* Synthesis and characterization of polyethylene glycol mediated silver nanoparticles by the green method. Int J Mol Sci 2012;13:6639-50.
4. Bhattacharya D, Gupta RK. Nanotechnology and potential of microorganisms. Crit Rev Biotechnol 2005;25:199-204.
5. Mohanpuria P, Rana NK, Yadav SK. Biosynthesis of nanoparticles: Technological concepts and future applications. J Nanopart Res 2008;10:507-17.
6. De D, Mandal SM, Gauri SS, Bhattacharya R, Ram S, Roy SK. Antibacterial effect of lanthanum calcium manganate (La0.67Ca0.33MnO3) nanoparticles against *Pseudomonas aeruginosa* ATCC 27853. J Biomed Nanotechnol 2010;6:138-44.
7. Dixon MB, Falconet C, Ho L, Chow CW, O'Neill BK, Newcombe G. Removal of cyanobacterial metabolites by nanofiltration from two treated waters. J Hazard Mater 2011;188:288-95.
8. Shameli K, Ahmad MB, Yunus WM, Rustaiyan A, Ibrahim NA, Zargar M, *et al.* Green synthesis of silver/montmorillonite/chitosan bionanocomposites using the UV irradiation method and evaluation of antibacterial activity. Int J Nanomedicine 2010;5:875-87.
9. Benelli G, Lo Iacono A, Canale A, Mehlhorn H. Mosquito vectors and the spread of cancer: An overlooked connection? Parasitol Res 2016;115:2131-7.
10. Govindarajan M, Benelli G. A facile one-pot synthesis of eco-friendly nanoparticles using *Carissa carandas*: Ovicidal and larvicidal potential on malaria, dengue and filariasis mosquito vectors. J Clust Sci 2017;28:15-36.
11. Vincent S, Kovendan K, Chandramohan B, Kamalakannan S, Kumar PM, Vasugi C, *et al.* Swift fabrication of silver nanoparticles using *Bougainvillea glabra*: Potential against the Japanese encephalitis vector, *Culex tritaeniorhynchus* giles (Diptera: Culicidae). J Clust Sci 2017;28:37-58.
12. Murugan K, Aarthi N, Kovendan K, Panneerselvam C, Chandramohan B, Kumar PM, *et al.* Mosquitocidal and antiplasmodial activity of *Senna occidentalis* (Cassiae) and *Ocimum basilicum* (Lamiaceae) from Maruthamalai hills against *Anopheles stephensi* and *Plasmodium falciparum*. Parasitol Res 2015;114:3657-64.
13. Gupta AK, Gupta M. Synthesis and surface engineering of iron oxide nanoparticles for biomedical applications. Biomaterials 2005;26:3995-4021.
14. Burtea C, Laurent S, Roch A, Vander Elst L, Muller RN. C-MALISA (cellular magnetic-linked immunosorbent assay), a new application of cellular ELISA for MRI. J Inorg Biochem 2005;99:1135-44.
15. Pardoe H, Clark PR, St Pierre TG, Moroz P, Jones SK. A magnetic resonance imaging based method for measurement of tissue iron concentration in liver arterially embolized with ferrimagnetic particles designed for magnetic hyperthermia treatment of tumors. Magn Reson Imaging 2003;21:483-8.
16. Dhavale RP, Waifalkar PP, Sharma A, Dhavale RP, Sahoo SC, Kollu P, *et al.* Monolayer grafting of aminosilane on magnetic nanoparticles: An efficient approach for targeted drug delivery system. J Colloid Interface Sci 2018;529:415-25.
17. Chourpa I, Douziech-Eyrolles L, Ngaboni-Okassa L, Fouquenet JF, Cohen-Jonathan S, Soucé M, *et al.* Molecular composition of iron oxide nanoparticles, precursors for magnetic drug targeting, as characterized by confocal Raman microspectroscopy. Analyst 2005;130:1395-403.
18. Kuppusamy P, Yusoff MM, Maniam GP, Govindan N. Biosynthesis of metallic nanoparticles using plant derivatives and their new avenues in pharmacological applications – An updated report. Saudi Pharm J 2016;24:473-84.
19. Adena SK, Upadhyay M, Vardhan H, Mishra B. Synthesis strategies and potential applications of gold nanoparticles in cancer theranostics: Labelling and visualizing, targeted drug delivery, photoablation therapy and sensing. Austin J Nanomed Nanotechnol 2018;6:1-11.
20. Seigneuric R, Markey L, Nuyten DS, Dubernet C, Evelo CT, Finot E, *et al.* From nanotechnology to nanomedicine: Applications to cancer research. Curr Mol Med 2010;10:640-52.
21. Huang J, Cao Y, Shao Q, Peng X, Guo Z. Magnetic nanocarbon adsorbents with enhanced hexavalent chromium removal: Morphology dependence of fibrillar vs particulate structures. Ind Eng Chem Res 2017;56:10689-701.
22. Kalantari K, Ahmad MB, Fard Masoumi HR, Shameli K, Basri M, Khandanlou R. Rapid and high capacity adsorption of heavy metals by Fe_3O_4/montmorillonite nanocomposite using response surface methodology: Preparation, characterization, optimization, equilibrium isotherms, and adsorption kinetics study. J Taiwan Inst Chem Eng 2015;49:192-8.
23. Lou X, Lin C, Luo Q, Zhao J, Wang B, Li J, *et al.* Crystal structure modification enhanced FeNb11O29 anodes for lithium-ion batteries. Chem Electro Chem 2017;4:3171-80.
24. Zhang L, Yu W, Han C, Guo J, Zhang Q, Xie H, *et al.* Large scaled synthesis of heterostructured electrospun Tio2/SnO2 nanofibers with an enhanced photocatalytic activity. J Electrochem Soc 2017;164:H651-6.
25. Liu T, Yu K, Gao L, Chen H, Wang N, Hao L, *et al.* A graphene quantum dot decorated SrRuO3 mesoporous film as an efficient counter electrode for high-performance dye-sensitized solar cells. J Mater Chem A 2017;5:17848-55.
26. Bagheri S, Chandrappa KG, Bee S, Hamid A. Generation of hematite nanoparticles via sol–gel method. Res J Chem Sci 2013;3:62-8.
27. Giri S, Samanta S, Maji S, Ganguli S, Bhaumik A. Magnetic properties of α-Fe2O3 nanoparticle synthesized by a new hydrothermal method. J Magn Magn Mater 2005;285:296-302.
28. Salazar-Alvarez G, Muhammed M, Zagorodni AA. Novel flow injection synthesis of iron oxide nanoparticles with narrow size distribution. Chem Eng Sci 2006;61:4625-33.
29. Abdullah NH, Shameli K, Abdullah EC, Abdullah LC. A facile and green synthetic approach toward fabrication of starch-stabilized magnetite nanoparticles. Chin Chem Lett 2017;28:1590-6.
30. Vijayakumar R, Koltypin Y, Felner I, Gedanken A. Sonochemical synthesis and characterization of pure nanometer-sized Fe_3O_4 particles. Mater Sci Eng 2000;286:101-5.
31. Carenza E, Barceló V, Morancho A, Montaner J, Rosell A, Roig A. Rapid synthesis of water-dispersible superparamagnetic iron oxide nanoparticles by a microwave-assisted route for safe labeling of endothelial progenitor cells. Acta Biomater 2014;10:3775-85.
32. Tartaj P, González-Carreño T, Serna CJ. From hollow to dense spheres: Control of dipolar interactions by tailoring the architecture in colloidal aggregates of superparamagnetic iron oxide nanocrystals. Adv Mater 2004;16:529-33.
33. Abedini A, Daud AR, Abdul Hamid MA, Kamil Othman N. Radiolytic formation of Fe3O4 nanoparticles: Influence of radiation dose on structure and magnetic properties. PLoS One 2014;9:e90055.
34. Vidal-Vidal J, Rivas J, López-Quintela MA. Synthesis of monodisperse maghemite nanoparticles by the microemulsion method. Colloids Surf A Physicochem Eng Aspects 2006;288:44-51.
35. Bomatí-Miguel O, Mazeina L, Navrotsky A, Veintemillas-Verdaguer S. Calorimetric study of maghemite nanoparticles synthesized by laser-induced pyrolysis. Chem Mater 2008;20:591-8.
36. Kim JH, Tratnyek PG, Chang YS. Rapid dechlorination of polychlorinated dibenzo-p-dioxins by bimetallic and nanosized zerovalent iron. Environ Sci Technol 2008;42:4106-12.
37. Wu W, He Q, Jiang C. Magnetic iron oxide nanoparticles: Synthesis and surface functionalization strategies. Nanoscale Res Lett 2008;3:397-415.
38. Thakkar KN, Mhatre SS, Parikh RY. Biological synthesis of metallic nanoparticles. Nanomedicine 2010;6:257-62.
39. Basavegowda N, Somai Magar KB, Mishra K, Lee YR. Green fabrication of ferromagnetic Fe_3O_4 nanoparticles and their novel catalytic applications for the synthesis of biologically interesting benzoxazinone and benzthioxazinone derivatives. New J Chem 2014;3:5415-20.
40. Basavegowda N, Mishra K, Lee YR. Sonochemically synthesized ferromagnetic Fe_3O_4 nanoparticles as a recyclable catalyst for the preparation of pyrrolo[3,4-c] quinoline-1,3-dione derivatives. RSC Adv 2014;4:61660-6.
41. Latha N, Gowri M. Biosynthesis and characterization of Fe_3O_4 nanoparticles using *Caricaya papaya* leaves extract. Int J Sci Res 2014;3:1551-6.
42. Venkateswarlu S, Rao YS, Balaji T, Prathima B, Jyothi NV. Biogenic synthesis of Fe_3O_4 magnetic nanoparticles using plantain peel extract. Mater Lett 2013;100:241-4.
43. Yew YP, Shameli K, Miyake M, Kuwano N, Bt Ahmad Khairudin NB, Bt Mohamad SE, *et al.* Green synthesis of magnetite (Fe_3O_4) nanoparticles using seaweed (*Kappaphycus alvarezii*) extract. Nanoscale Res Lett 2016;11:276.
44. Rosi NL, Giljohann DA, Thaxton CS, Lytton-Jean AK, Han MS, Mirkin CA. Oligonucleotide-modified gold nanoparticles for intracellular gene regulation. Science 2006;312:1027-30.
45. Maldini M, Sosa S, Montoro P, Giangaspero A, Balick MJ, Pizza C, *et al.* Screening of the topical anti-inflammatory activity of the bark of *Acacia cornigera* Willdenow, *Byrsonima crassifolia* Kunth, *Sweetia panamensis* Yakovlev and the leaves of *Sphagneticola trilobata* Hitchcock. J Ethnopharmacol 2009;122:430-3.
46. Kade IJ, Barbosa NB, Ibukun EO, Igbakin AP, Nogueira CW, Rocha JB. Aqueous extracts of *Sphagneticola trilobata* attenuates streptozotocin-induced hyperglycaemia in rat models by modulating oxidative stress parameters. Biol Med 2010;2:1-13.
47. Verma RS, Padalia RC, Chauhan A, Sundaresan V. Essential oil composition of *Sphagneticola trilobata* (L.) Pruski from India. J Essent Oil Res 2014;26:29-33.
48. Ren H, Dong L, Zhou Z, Xu Q, Tan J. Chemical constituents from *Sphagneticola trilobata*. J Chin Med Mater 2015;38:1426-9.

49. Vinay SP, Chandrasekhar N, Chandrappa CP. Eco-friendly approach for the green synthesis of silver nanoparticles using flower extracts of *Sphagneticola trilobata* and study of antibacterial activity. Int J Pharm Biol Sci 2018;7:145-52.
50. Wang H, Helliwell K, You X. Isocratic elution system for the determination of catechins, caffeine and gallic acid in green tea using HPLC. Food Chem 2000;68:115-21.
51. Wang T, Jin X, Chen Z, Megharaj M, Naidu R. Green synthesis of Fe nanoparticles using eucalyptus leaf extracts for treatment of eutrophic wastewater. Sci Total Environ 2014;466-467:210-3.
52. Hariani PL, Faizal M, Ridwan R, Marsi M, Setiabudidaya D. Synthesis and properties of Fe_3O_4 nanoparticles by co precipitation method to removal procion dye. IJESD 2013;4:336-40.
53. Hussein-Al-Ali SH, El Zowalaty ME, Hussein MZ, Geilich BM, Webster TJ. Synthesis, characterization, and antimicrobial activity of an ampicillin-conjugated magnetic nanoantibiotic for medical applications. Int J Nanomedicine 2014;9:3801-14.
54. Shimamura T, Sumikura Y, Yamazaki T, Tada A, Kashiwagi T, Ishikawa H, *et al*. Applicability of the DPPH assay for evaluating the antioxidant capacity of food additives – Inter-laboratory evaluation study. Anal Sci 2014;30:717-21.
55. Karade VC, Dongale TD, Sahoo SC, Kollu P, Chougale AD, Patil PS, *et al.* Effect of reaction time on structural and magnetic properties of green-synthesized magnetic nanoparticles. J Phys Chem Solids 2018;120:161-6.
56. Gholoobi A, Meshkat Z, Abnous K, Ghayour-Mobarhan M, Ramezani M, Homaei Shandiz F, *et al*. Biopolymer-mediated synthesis of Fe_3O_4 nanoparticles and investigation of their *in vitro* cytotoxicity effects. J Mol Struct 2017;1141:594-9.